A quantum walk model with energy dissipation for a dressed-photon–phonon confined by an impurity atom-pair in a crystal

M. Ohtsu[1], E. Segawa[2], K. Yuki[3], and S. Saito[4]

[1]Research Origin for Dressed Photon,3-13-19 Moriya-cho, Kanagawa-ku, Yokohama, Kanagawa 221-0022, Japan

[2]Yokohama National University, 79-8 Tokiwadai, Hodogaya-ku, Yokohama, Kanagawa 240-8501, Japan

[3]Middenii, 3-3-13 Nishi-shinjuku, Sinjuku-ku, Tokyo 160-0023, Japan

[4]Kogakuin University, 2665-1, Nakano-machi, Hachioji, Tokyo 192-0015, Japan

Abstract

This paper introduces the energy dissipation constant κ into a two-dimensional QW model for describing the intrinsic features of dressed-photon–phonon creation and confinement in a B atom-pair in a Si crystal. It succeeded in describing unique features, including: (a) The magnitude of the energy dissipated from the B atom-pair took the maximum at κ=0.2; (b) the total dissipated energy over the whole volume of the Si crystal monotonically increased with κ, whereas the energy of the source of dissipation complementarily decreased; and (c) the dissipated energy exhibited the feature of photon breeding with respect to the photon momentum. From these features, it was confirmed that the intrinsic features of microscopic and macroscopic fields were successfully described in a consistent manner.

1. Introduction

A dressed photon (DP) is a quantum field created by the interaction between photons and electrons (or excitons) in a nanometer-sized particle (NP). The created DP localizes at the NP. It is an off-shell field because its momentum has a large uncertainty due to its subwavelength size [1,2]. Furthermore, the DP couples with a phonon to create a new quantum field, named a dressed-photon–phonon (DPP). By using a two-dimensional quantum walk (QW) model, ref. [3] analyzed the spatial distribution of a DPP that was confined by an impurity boron (B) atom-pair in a silicon (Si) crystal. This analysis found that the DPP was efficiently confined by the B atom-pair when the pair was oriented along a direction perpendicular to that of the incident light propagation.

Here, it should be pointed out that the experiments measured not the energy of the DPP itself confined in the B atom-pair but the on-shell energy that leaked out from the Si crystal. This energy was created due to the dissipation of the off-shell DPP field energy. For comparison with experimental results, this paper introduces the phenomenological dissipation constant κ into the QW model [4].

Section 2 presents equations for the QW model without and with energy dissipation. Section 3 reports the results of numerical calculations. Section 4 discusses the origins of why the present QW

model was effective in describing intrinsic features of the DPP energy transfer that agreed with experimental results. Section 5 presents a summary.

2. Equations for the QW model

The first part of this section presents equations for the QW model without energy dissipation. This is a brief review of the formulation given in ref. [3]. The second part presents novel equations to deal with the energy dissipation.

2.1. Without energy dissipation

The square lattice in Fig. 1(a) was used in ref. [3] for a two-dimensional QW model without energy dissipation. By radiating light (an input signal that propagates along the $+y$-axis) to the lower side of this lattice, DPs are created at the sites in the lattice and travel in the upper-right or lower-left directions. These directions correspond to directions parallel and antiparallel (along the $+y$ and $-y$ axes, respectively) to the direction of the irradiated light propagation. Since the QW model deals with the DP hopping to the nearest-neighbor site, these directions are represented by red and blue bent arrows, respectively, in Figs. 1(b) and (c). The phonon is represented by a green closed loop because it does not hop due to its nonlocalized nature.

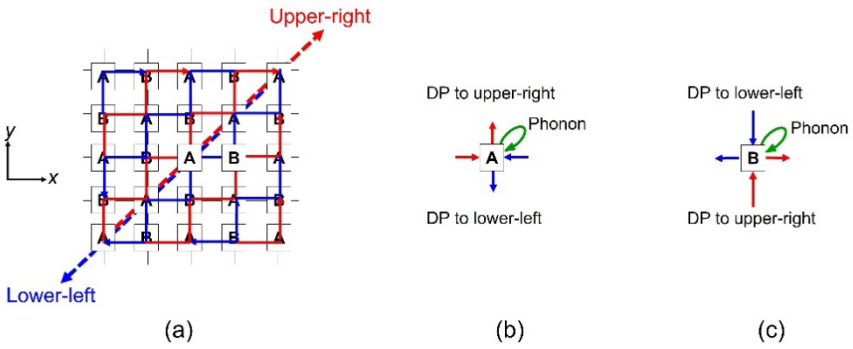

Fig. 1 Two-dimensional square lattice.

(a) DPs that travel in the upper-right and lower-left directions. They are represented by bent red and blue arrows, respectively.

(b) and (c) The magnified figure at sites A and B in (a), respectively. The green loop represents a phonon.

Since the DPP is created as a result of coupling between two counter-travelling DPs and a phonon, a three-dimensional vector

$$\vec{\psi}_{t,(x,y)} = \begin{bmatrix} y_{DP+} \\ y_{DP-} \\ y_{Phonon} \end{bmatrix}_{t,(x,y)} \tag{1}$$

is used to represent its creation probability amplitude, where [ ] is the vector at time t and at the position of the lattice site (x, y), y_{DP+} and y_{DP-} are the creation probability amplitudes of the DPs that travel by repeating the hopping in the upper-right and lower-left directions, respectively, and y_{Phonon} is that of the phonon.

First, the spatial-temporal evolution equation for the DPP, hopping out from the site A in Fig. 1(b), is given by

$$\vec{\psi}_{t,(x,y)\updownarrow} = P_+\vec{\psi}_{t-1,(x-1,y)\rightarrow} + P_-\vec{\psi}_{t-1,(x+1,y)\leftarrow} + P_0\vec{\psi}_{t-1,(x,y)\circ}\,. \tag{2}$$

The vector $\vec{\psi}_{t,(x,y)\updownarrow}$ on the left-hand side is composed of two DPs ($y_{DP+\uparrow}$ and $y_{DP-\downarrow}$: hopping out along the $\pm y$ axes) and a phonon ($y_{Phonon\circ}$) at time t. The right-hand side is composed of two DPs ($y_{DP+\rightarrow}$ and $y_{DP-\leftarrow}$: hopping into site A along the $\pm x$ axes) and a phonon ($y_{Phonon\circ}$). The three matrices on the right-hand side are

$$P_+ = \begin{bmatrix} \varepsilon_+ & J & \chi \\ 0 & 0 & 0 \\ 0 & 0 & 0 \end{bmatrix}, \tag{3a}$$

$$P_- = \begin{bmatrix} 0 & 0 & 0 \\ J & \varepsilon_- & \chi \\ 0 & 0 & 0 \end{bmatrix}, \tag{3b}$$

and

$$P_0 = \begin{bmatrix} 0 & 0 & 0 \\ 0 & 0 & 0 \\ \chi & \chi & \varepsilon_0 \end{bmatrix}. \tag{3c}$$

Diagonal elements ε_+ and ε_- are the eigen-energies of the DPs (y_{DP+} and y_{DP-}), respectively, and ε_0 is that of the phonon. Off-diagonal elements J and χ represent the DP hopping energy and the DP-phonon coupling energy, respectively.

Second, the spatial-temporal evolution equation for the DPP, hopping out from the site B in Fig. 1(c), is given by

$$\vec{\psi}_{t,(x,y)\leftrightarrow} = P_+\vec{\psi}_{t-1,(x,y-1)\uparrow} + P_-\vec{\psi}_{t-1,(x,y+1)\downarrow} + P_0\vec{\psi}_{t-1,(x,y)\circ} \tag{4}$$

The vector $\vec{\psi}_{t,(x,y)\leftrightarrow}$ on the left-hand side is composed of two DPs ($y_{DP+\rightarrow}$ and $y_{DP-\leftarrow}$: hopping out along the $\pm x$ axes) and a phonon ($y_{Phonon\circ}$) at time t. The right-hand side is composed of two DPs ($y_{DP+\uparrow}$ and $y_{DP-\downarrow}$: hopping into the site B along the $\pm y$ axes) and a phonon ($y_{Phonon\circ}$). The three matrices of eqs.3(a) – (c) are used also in eq. (4).

By using vectors

$$\left[\vec{\psi}_{t,(x,y)\leftrightarrow}\right] \equiv \begin{bmatrix} y_{DP+\rightarrow} \\ y_{DP-\leftarrow} \\ y_{Phonon\circ} \end{bmatrix}_{t,(x,y)} \tag{5a}$$

and

$$\left[\vec{\psi}_{t,(x,y)\updownarrow}\right] \equiv \begin{bmatrix} y_{DP+\uparrow} \\ y_{DP-\downarrow} \\ y_{Phonon\circ} \end{bmatrix}_{t,(x,y)}, \tag{5b}$$

eqs. (2) and (4) are lumped together and represented by

$$\vec{\psi}_{t,(x,y)} = \begin{bmatrix} \left[\vec{\psi}_{t,(x,y)\leftrightarrow}\right] \\ \left[\vec{\psi}_{t,(x,y)\updownarrow}\right] \end{bmatrix} = \begin{bmatrix} [0] & U \\ U & [0] \end{bmatrix} \begin{bmatrix} \left[\vec{\psi}_{t-1,(x,y)\leftrightarrow}\right] \\ \left[\vec{\psi}_{t-1,(x,y)\updownarrow}\right] \end{bmatrix}, \tag{6}$$

where

$$U \equiv P_+ + P_- + P_0 = \begin{bmatrix} \varepsilon_+ & J & \chi \\ J & \varepsilon_- & \chi \\ \chi & \chi & \varepsilon_0 \end{bmatrix}, \tag{7}$$

and

$$[0] \equiv \begin{bmatrix} 0 & 0 & 0 \\ 0 & 0 & 0 \\ 0 & 0 & 0 \end{bmatrix}. \tag{8}$$

One can easily recognize from eq. (6) that the two DPs (y_{DP+} and y_{DP-}) follow zigzag-shaped routes (represented by bent red and blue arrows).

Since the DP couples with the phonon preferably at the B atom site, χ / J has to be larger than unity. Here, it is fixed to 20, as was confirmed in ref. [5]. On the other hand, $\chi = J$ at the Si atom sites.

2.2. With energy dissipation

The square lattice in Fig. 1(a) is also used for introducing energy dissipation to the QW model. For this introduction, the three-dimensional vector of eq. (1) is replaced by a four-dimensional vector

$$\vec{\psi}'_{t,(x,y)} = \begin{bmatrix} y_{DP+} \\ y_{DP-} \\ y_{Phonon} \\ y_{dis} \end{bmatrix}_{t,(x,y)}. \tag{9}$$

The fourth line y_{dis} represents the creation probability amplitude of the energy dissipated from the square lattice. The spatial-temporal evolution equation of eq. (6) is represented by

$$\vec{\psi}'_{t,(x,y)} = \begin{bmatrix} \left[\vec{\psi}'_{t,(x,y)\leftrightarrow}\right] \\ \left[\vec{\psi}'_{t,(x,y)\updownarrow}\right] \\ \left[\vec{\psi}''_{t,(x,y),dis}\right] \end{bmatrix} = \begin{bmatrix} [0] & \sqrt{1-\kappa^2}U & [0] \\ \sqrt{1-\kappa^2}U & [0] & [\kappa] \\ [0] & [\kappa] & [0] \end{bmatrix} \begin{bmatrix} \left[\vec{\psi}'_{t-1,(x,y)\leftrightarrow}\right] \\ \left[\vec{\psi}'_{t-1,(x,y)\updownarrow}\right] \\ \left[\vec{\psi}''_{t-1,(x,y),dis}\right] \end{bmatrix}. \tag{10}$$

The third line of the left-hand side vector corresponds to the dissipated energy

$$\left[\vec{\psi}''_{t,(x,y),dis}\right] \equiv \begin{bmatrix} y_{DP+,dis} \\ y_{DP-,dis} \\ y_{Phonon\bigcirc} \end{bmatrix}_{t,(x,y)} . \tag{11}$$

The first and second lines ($y_{DP+,dis}$ and $y_{DP-,dis}$) in eq. (11) represent the dissipated energies that travel along the directions parallel and anti-parallel to that of the irradiated light, respectively. Their sources are y_{DP+} and y_{DP-} in eq. (9), respectively. The phonon ($y_{Phonon,\bigcirc}$) does not contribute to the energy dissipation due to its non-travelling nature.

The quantity κ in the matrix

$$[\kappa] \equiv \begin{bmatrix} \kappa & 0 & 0 \\ 0 & \kappa & 0 \\ 0 & 0 & 0 \end{bmatrix} \tag{12}$$

on the right-hand side of eq. (10) is a phenomenological dissipation constant $(0 \le \kappa \le 1)$. The quantity $\sqrt{1-\kappa^2}$ represents the magnitude of the energy left in the square lattice after energy dissipation.

3. Calculated results

Numerical calculations were carried out for the case of the B atom-pair oriented along the x-axis. Its length d was fixed to $3a$ (a is the lattice constant of the Si crystal) because experiments have confirmed that this length was most efficient for creating and confining the DPP in the B atom-pair, and also because it is advantageous for evaluating asymmetric features of the spatial distribution of the DPP creation probability in Subsection 3.2. The creation probability C_{av}, averaged over all the sites in the B atom-pair, was used for evaluating the magnitude of the confinement. It is defined in ref. [3] as $C_{av} \equiv A_{av} - B_{av}$. Here, A_{av} is the creation probability, averaged over the Si atoms in the B

atom-pair. B_{av} is the average for the sites of the two B atoms. Although ref. [5] claimed that the number n of the sites on the side of the square lattice must be equal to or higher than 51, in the present paper, n is fixed to 21 for shortening the calculation time of the computer system we used (refer to the Appendix).

3.1. The optimum value of the dissipation constant

Figure 2(a) shows the relation between κ and C_{av} of the energy that dissipated and leaked out from the square lattice to the external space. It is the magnitude of the dissipated energy $y_{DP+,dis}$ in eq. (11) that travels along the direction parallel to that of the irradiated light propagation ($+y$-axis). In Fig. 2(b), A_{av} is also used to represent the relation above. These figures show that C_{av} and A_{av} take the maximum at κ=0.2 ($\equiv \kappa_{opt}$). The existence of such an optimum value κ_{opt} agrees with experimental results and implies the feature of "comfortability" that has been studied using the QW model [6]. In the discussions above, only $y_{DP+,dis}$ was dealt with because its magnitude was much larger than that of $y_{DP-,dis}$, as will be shown in Figs. 7 and 8 in Subsection 3.2.

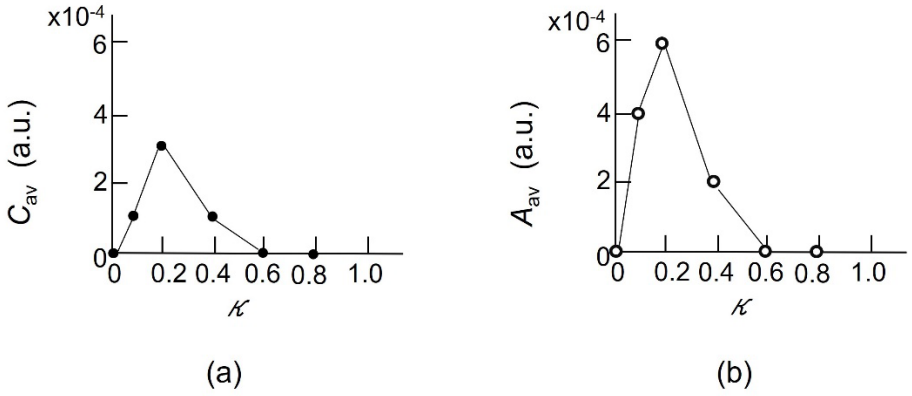

Fig. 2 Relation between κ and the magnitude of the dissipated energy $y_{DP+,dis}$.
(a) and (b) are represented by using C_{av} and A_{av} at the sites in the B atom-pair, respectively.

Figures 3(a) and (b) show the relation between κ and the magnitude of the energy of the source of dissipation. Since the relations in Figs. 2(a) and (b) show the convex upward-feature, it is

expected that Figs. 3(a) and (b) complementarily show the convex downward-feature to meet the energy conservation requirement. However, they show a monotonic decrease with κ.

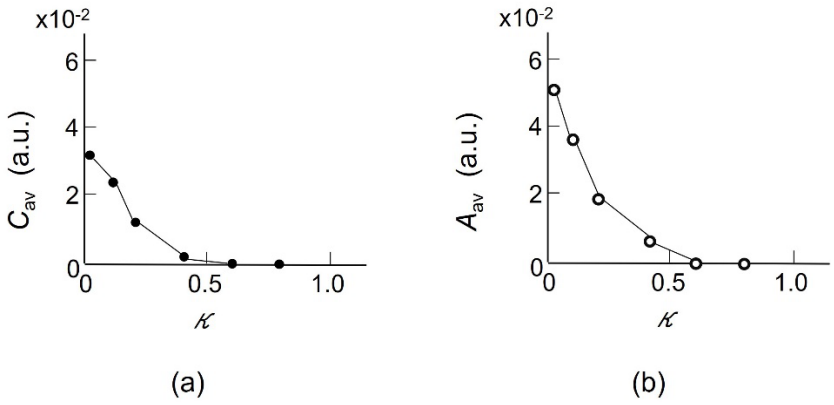

Fig. 3 Relation between κ and the source of the energy of dissipation.
(a) and (b) are represented by using C_{av} and A_{av} at the sites in the B atom-pair, respectively.

The origin of this monotonic decrease is that Figs. 2 and 3 were derived by calculating the magnitudes of the energy only at the sites in the B atom-pair. However, since the dissipated energy is the on-shell field energy that emerges from the off-shell field, it spreads over the whole volume of the Si crystal and finally leaks out from the Si crystal. Thus, in order to confirm the complementary feature between Figs. 2 and 3, the magnitude of the total energy must be calculated by summing up over all the sites of the square lattice.

Figure 4(a) shows such total dissipated energy, where the values of A_{av} were normalized to that of κ=1. This figure shows that A_{av} monotonically increases with κ, which implies that the total dissipated energy increases with the increase of κ and spreads over the whole volume of the Si crystal. This spread corresponds to diffraction, which is an intrinsic feature of the on-shell field in a visible macroscopic space. Figure 4(b) represents the values of A_{av} for the total energy of the source of dissipation, where A_{av} is normalized to that of κ=0. It shows that A_{av} monotonically decreases with κ. By comparing Figs. 4(a) and (b), the complimentary feature was successfully confirmed.

In contrast to the complimentary feature in the visible macroscopic space above, the existence of the optimum value κ_{opt} in Fig. 2 implies the intrinsic feature of the off-shell DPP field in an invisible microscopic space. By this contrast, it is confirmed that the present QW model with energy dissipation could successfully describe the intrinsic features of invisible microscopic and visible macroscopic spaces in a consistent manner.

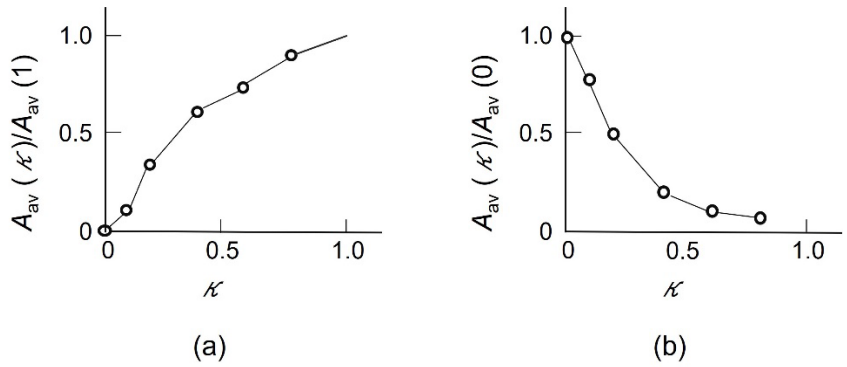

Fig. 4 Relation between κ and the total energy.

(a) The total dissipated energy, where A_{av} is normalized to that of κ =1.

(b) The total energy of the source of dissipation, where A_{av} is normalized to that of κ =0.

3.2. Photon breeding with respect to momentum

Reference [3] discussed the photon breeding (PB) with respect to the photon momentum by using the asymmetric spatial distribution of the DPP creation probability as a clue. On the other hand, since experiments were performed to evaluate the characteristics of the light that leaked out from the Si crystal for discussing PB, this Subsection uses the QW model with energy dissipation for a more detailed comparison with experimental results than that of ref. [3].

First, Fig. 5(a) shows the distribution of the DPP creation probability at the sites in the B atom-pair without energy dissipation, which agrees with that of Fig. 5(d) in ref. [3] (d / a =3). Figures 5(b) – (d) are those for y_{DP+}, y_{DP-}, and y_{Phonon}, respectively, which are the constituent elements of the DPP. In the case of y_{DP+} (Fig. 5(b)), the probability at the right site of the Si atom is larger than that at the left site. On the contrary, the probability of y_{DP-} (Fig. 5(c)) is larger at the left site. Figure 5(d) shows the symmetric feature. Due to the asymmetric features in Figs. 5(b) and (c) above, the probability in Fig. 5(a) is asymmetric. These features agree with those of Figs. 10(a) – (c) in ref. [3] (d / a =3). Figures 6(a) – (d) show the calculated results of the probability with energy dissipation (κ =0.2). Their asymmetric features agree with those of Figs. 5(a) – (d) even though the probabilities are smaller due to the dissipation.

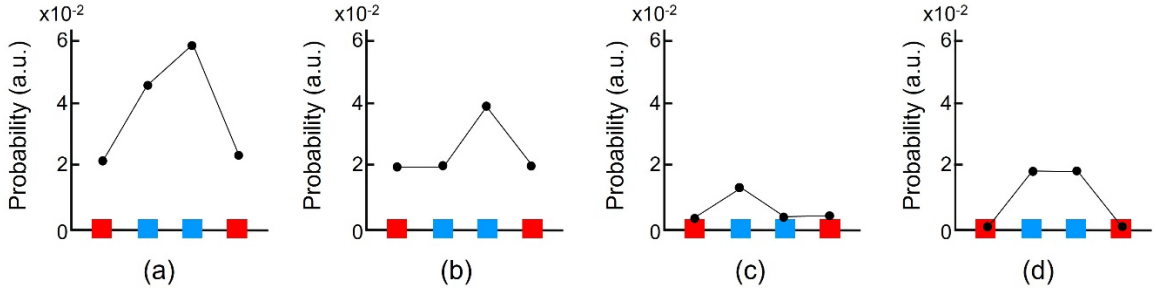

Fig. 5 Creation probability at the sites in the B atom-pair (d/a=3) without energy dissipation.

(a) DPP, (b) y_{DP+}, (c) y_{DP-} and (d) y_{Phonon}. Red and blue squares represent the sites of the B and Si atoms, respectively.

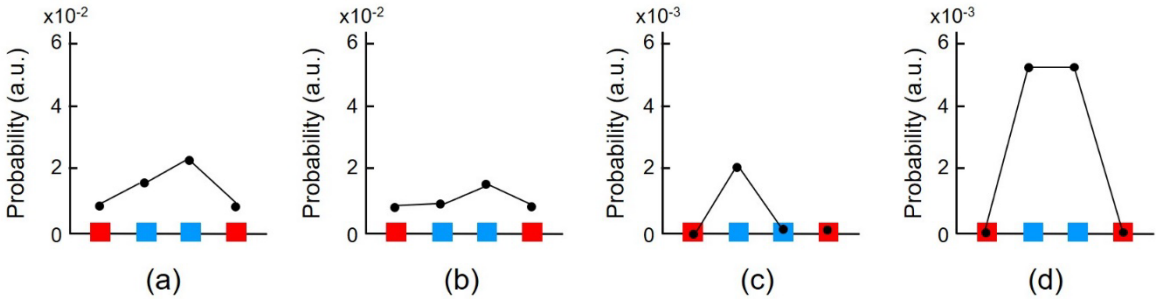

Fig.6 Creation probability at the sites in the B atom-pair (d/a=3) with energy dissipation (κ=0.2).

(a) DPP, (b) y_{DP+}, (c) y_{DP-} and (d) y_{Phonon}. Red and blue squares represent the sites of the B and Si atoms, respectively.

Second, Fig. 7(a) shows the probability for the dissipated energy $y_{DP+,dis}$ (κ=0.2). This figure shows that the probability at the right site of the Si atom is larger than that at the left site, as was the case in Fig. 6(a). Figure 7(b) is for the dissipated energy $y_{DP-,dis}$ (κ=0.2) whose probability at the left site of the Si atom is larger than that at the right site, as was the case of Fig. 6(b). Here, it should be noted that the probability in Fig. 7(a) is much larger than that in Fig. 7(b). That is, the magnitude of the dissipated energy $y_{DP+,dis}$ (traveling in the direction parallel to that of the incident light) is much larger than that of $y_{DP-,dis}$ (traveling in the anti-parallel direction). It implies that the momentum of the photon, created due to the dissipation and leaked out from the Si crystal, is equivalent to that of the incident light. This equivalence manifests the PB with respect to the photon momentum.

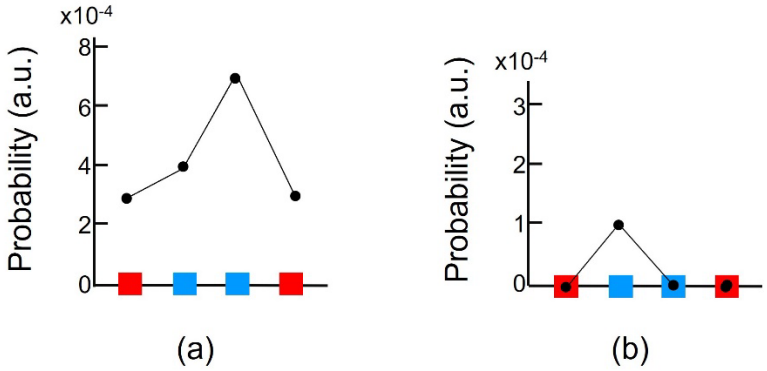

Fig. 7 Creation probability of the dissipated energy (κ =0.2) at the sites in the B atom-pair.
(a) and (b) are the dissipated energies $y_{DP+,dis}$ and $y_{DP-,dis}$, respectively.
Red and blue squares represent the sites of the B and Si atoms, respectively.

Finally, Figures 8(a) and (b) show the relations between κ and the creation probabilities of the dissipated energies $y_{DP+,dis}$ and $y_{DP-,dis}$ in eq. (11), which travel in the directions parallel and anti-parallel to that of the incident light, respectively. The values of C_{av} and A_{av} for $y_{DP+,dis}$ (Fig. 8(a)) are larger than those for $y_{DP-,dis}$ (Fig. 8(b)), which represents the PB with respect to the photon momentum, as was indicated in Fig. 7. For reference, the values of C_{av} and A_{av} in Figs. 8(a) and (b) take the maxima at κ=0.2, which is in agreement with Fig. 2.

From a discussion of Figs. 7 and 8, it is concluded that the PB with respect to the photon momentum was successfully confirmed by the QW model with energy dissipation.

4. Discussions

As reported in Ref. [4], it was confirmed that the calculated results of the DPP creation probability at the tip of a fiber probe agreed with experimental results. Furthermore, in the present paper, we showed that the calculated results in Section 3 agreed with the experimental results. These two agreements imply that the QW model is effective for describing the intrinsic features of the DPP energy transfer. This effectiveness is attributed to two origins:

(1) Non-commutativity: The QW model is based on non-commutative algebra using vectors and matrices. On the other hand, the DP is a quantum field that mediates the non-commutative interaction between nanometer-sized particles (NP). Thus, one origin of the effectiveness noted above is attributed to the non-commutative aspect that is common to the QW and DP.

(2) Localization: The QW model treats the energy transfer from one site to its nearest-neighbor site, both of which represent local positions in the QW lattice. On the other hand, since the DP is a localized field [7], its quantum mechanical position operator can be defined. Thus, if the NP is considered as the site of the QW model, the position of the DP is identified with that of this site. This implies that the other origin of the effectiveness noted above is the localization aspect that is common to the QW and DP.

At the end of this section, it should be pointed out that the constant κ is a phenomenological quantity that was introduced to analyze the energy dissipation. It is expected that its identity can be revealed by future studies of classical and quantum measurement theories [8].

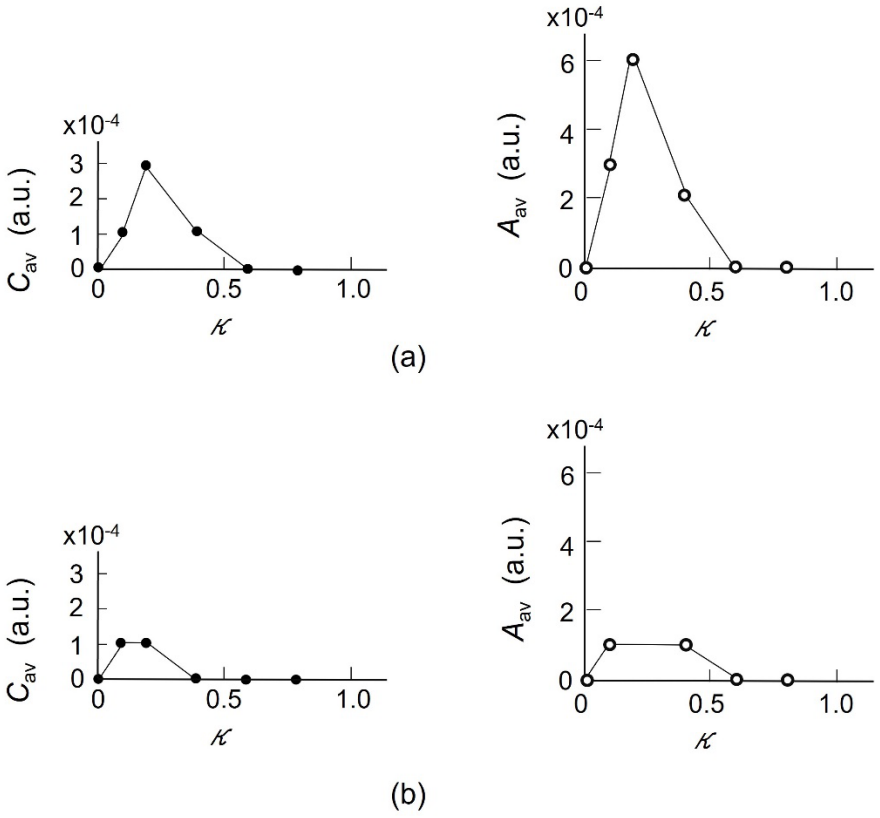

Fig. 8 The relations between κ and the creation probability of the dissipated energy.
(a) and (b) are for $y_{DP+,dis}$ and $y_{DP-,dis}$, respectively.

5. Summary

The present paper introduced an energy dissipation constant κ into the two-dimensional QW model of ref. [3] for detailed analysis of the DPP creation and confinement by a B atom-pair in a Si crystal. As a result, it succeeded in describing the intrinsic features of the DPP energy transfer, including:
(a) The magnitude of the energy dissipated from the B atom-pair took a maximum at κ=0.2.
(b) The total dissipated energy over the whole volume of the Si crystal monotonically increased with

κ. On the other hand, the total energy of the source of dissipation complementarily decreased.
(c) The dissipated energy exhibited the feature of photon breeding (PB) with respect to the photon momentum.

Among the features above, (a) implies localization of the DPP, which is an intrinsic feature of an off-shell field in a microscopic space. In contrast, (b) represents the feature of the dissipated energy of the macroscopic on-shell field. It was confirmed from these contrasting features that the intrinsic features of microscopic and macroscopic fields were successfully described by introducing the energy dissipation into the QW model in a consistent manner.

Appendix Dependence on the number of lattice sites

Although ref. [5] has pointed out that the number n of the sites on the side of the two-dimensional lattice should be equal to or higher than 51 to ensure sufficiently high accuracy of numerical calculations, it was fixed to 21 in the present calculation to shorten the calculation time with the computer system currently used. In order to show specific evidence why it is permissible to use the smaller value of n (=21), this Appendix demonstrates representative results of calculation for n =51. They are the results for the case of κ =0.2 ($\equiv \kappa_{opt}$).

Figures A1(a)-(d) show the calculated results (n =51) corresponding to Figs. 6(a)-(d) (n =21). It is easily found that the spatial distribution profile of the creation probabilities in Figs. A1 and 6 are equivalent. The only difference is that the values on the vertical axes in Fig. A1 are 1/10 times those of Fig. 6. However, this is reasonable because the total number of sites for n =51 is 10 times that for n =21. Furthermore, Figs. A2(a) and (b) show the calculated results (n =51) corresponding to Figs. 7(a) and (b) (n =21). As is the case above, the spatial distribution profiles of the creation probabilities in Figs. A2 and 7 are also equivalent. Here, the values of the vertical axes in Fig. A2 are also 1/10 those of Fig. 7 also due to the reasonable origin described above. A technical advantage was that the computation time for n =21 was as short as 1/10 that for n =51.

By comparing these figures, it is concluded that the calculated results for n =21 and n =51 are equivalent to each other. The origins of this equivalence are: In the case of a fiber probe, a complicated triangular lattice was required, and the reflection of the DPP had to be taken into account at the slope of the triangle [5]. In contrast, a simpler square lattice was accepted in the present study. In addition, it was permissible to neglect the reflection at the sides of the square lattice, as was verified in ref. [4].

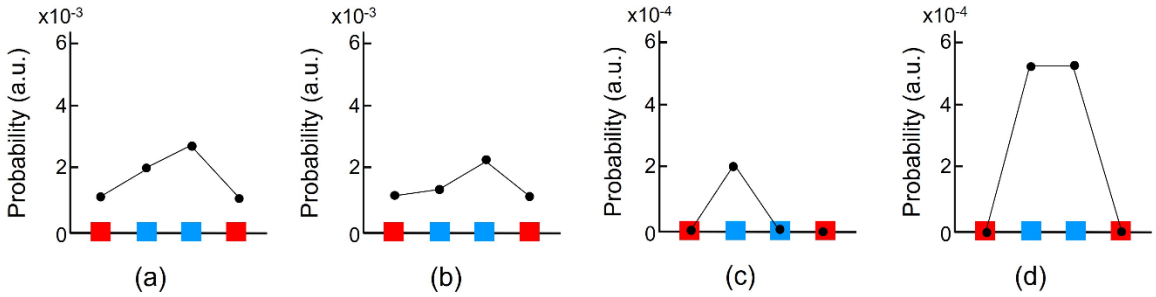

Fig.A1 Creation probability at the sites in the B atom-pair (d / a =3) with energy dissipation (κ =0.2).

Here, n is fixed to 51. (a) DPP, (b) y_{DP+}, (c) y_{DP-} and (d) y_{Phonon}.

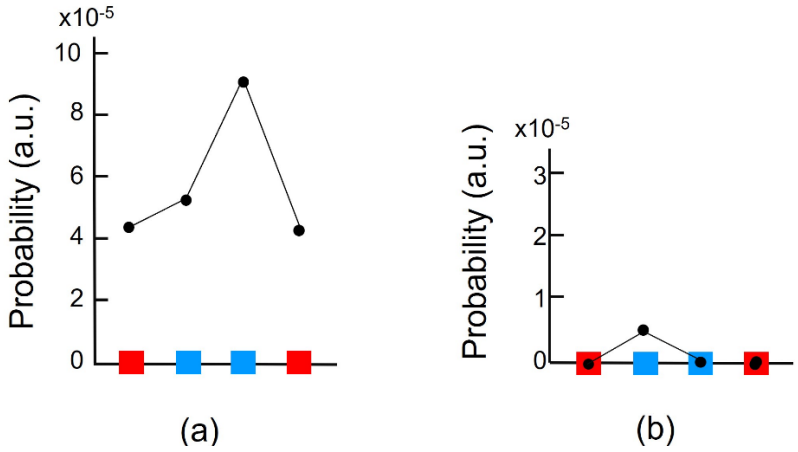

Fig. A2 Spatial profile of the probability for the dissipated energy (κ =0.2).

Here, n is fixed to 51. (a) and (b) are the dissipated energies $y_{DP+,dis}$ and $y_{DP-,dis}$, respectively.

References

[1] Ohtsu, M., Ojima, I., and Sakuma, H., "Dressed Photon as an Off-Shell Quantum Field," *Progress in Optics* Vol.64, (ed. T.D. Visser) pp.45-97 (Elsevier, 2019).

[2] Ohtsu,M., *Off-Shell Applications In Nanophotonics*, Elsevier, Amsterdam (2021) p.5.

[3] Ohtsu, M., Segawa, E., Yuki, K., and Saito, S., "Spatial distribution of dressed-photon–phonon confined by an impurity atom-pair in a crystal," *Off-shell Archive* (January, 2023) OffShell: 2301O.001.v1., **DOI** 10.14939/2301O.001.v1 https://rodrep.or.jp/en/off-shell/original_2301O.001.v1.html

[4] Ohtsu, M., Segawa, E., and Yuki, K., "Quantum walk analyses of the dressed photon confinement by an impurity atom pair," Abstracts of the 70th Jpn. Soc. Appl. Phys. Spring Meeting, March 15-18, 2023, (Sophia Univ. and Online meeting), paper number 16a-A201-4 (in Japanese).

[5] Ohtsu, M., Segawa, E., Yuki, K., and Saito, S., ""Dressed-photon—phonon creation probability on the tip of a fiber probe calculated by a quantum walk model," *Off-shell Archive* (December, 2022) OffShell: 2212O.001.v1.,

DOI 10.14939/2212O.001.v1., https://rodrep.or.jp/en/off-shell/original_2212O.001.v1.html

[6] Higuchi, K., Komatsu, T., Konno, N., Morioka, H., and Segawa, H., "A Discontinuity of the Energy of Quantum Walk in Impurities," *Symmetry* **2021**,13, 1134. https://doi.org/10.3390/sym13071134

[7] Sakuma, H. and Ojima, I., "On the Dressed Photon Constant and Its Implication for a Novel Perspective on Cosmology," *Symmetry* **2021**, 13, 593. https://doi.org/10.3390/sym13040593

[8] Okamura, K., "Towards a Measurement Theory for Off-Shell Quantum Fields," *Symmetry* **2021**, 13, 1183. https://doi.org/10.3390/sym13071183